Nanoparticle uptake and their co-localization with cell compartments - a confocal Raman microscopy study at single cell level

I Estrela-Lopis[1], G Romero[2], E Rojas[2], S E Moya[2] and E Donath[1]

[1]Institute of Medical Physics and Biophysics, Leipzig University, Härtelstraße 16, 04107 Leipzig, Germany

[2]CIC biomaGUNE, Paseo Miramón 182 Edificio Empresarial C, 20009 San Sebastián, Gipuzkoa, Spain.

E-mail: Irina.Estrela-Lopis@medizin.uni-leipzig.de

Abstract. Confocal Raman Microscopy, a non-invasive, non-destructive and label-free technique, was employed to study the uptake and localization of nanoparticles (NPs) in the Hepatocarcinoma human cell line HepG2 at the level of single cells. Cells were exposed to carbon nanotubes (CNTs) the surface of which was engineered with polyelectrolytes and lipid layers, aluminium oxide and cerium dioxide nanoparticles. Raman spectra deconvolution was applied to obtain the spatial distributions of NPs together with lipids/proteins in cells. The colocalization of the NPs with different intracellular environments, lipid bodies, protein and DNA, was inferred. Lipid coated CNTs associated preferentially with lipid rich regions, whereas polyelectrolyte coated CNTs were excluded from lipid rich regions. Al_2O_3 NPs were found in the cytoplasm. CeO_2 NPs were readily taken up and have been observed all over the cell. Raman z-scans proved the intracellular distribution of the respective NPs.

1. Introduction

Nanotechnology has seen a rapid development in recent years. Novel products appeared at the market ahead of that nanoparticle and nanomaterials related ecological and health risks have been addressed by the respective regulations. A proper risk management of nanomaterials requires more information on the human and ecological effects of exposure to various nanomaterials [1]. Understanding the effects of nanoparticles (NPs) and nanostructured materials on human health (and ecology) is thus an issue of major importance [2]. Studies with cell culture model systems may contribute to the understanding of the effect of nanoparticles on human health [3].

In contrast to toxicity at the molecular level, where toxic compounds directly interfere with the metabolism, the toxicity of NPs may be caused by the interaction of the NPs with various cellular components. NPs may interfere with the complex intracellular machinery by disturbing the conformation of cellular constituents, the intracellular hierarchy and transport routes. For a deeper understanding of the mechanism of the interaction of NPs with biological matter it is therefore desirable to study the localization of NPs within cells and organs. However, the possibilities to monitor NPs at the cellular level are limited. Fluorescent techniques as a rule require labeling, which, given the small size of the nanoparticles, may seriously interfere with their properties. Electron

microscopy has an excellent resolution but it is time consuming and restricted to the analysis of a limited number of images.

An alternative technique capable of measuring the presence and distribution of NPs and nanostructured materials in cells is Raman Microscopy, since a wide variety of NPs and nanostructures shows Raman active vibration modes. A powerful nonlinear Raman spectroscopy technique is the Coherent Anti-Stokes Raman Scattering (CARS) technique. The anti-Stokes signal is significantly enhanced by means of focusing the excitation energy on a single Raman band. This permits, combined with confocal microscopy, the imaging of cells within a very short time [4]. The drawbacks of CARS are the lack of spectral information and the presence of nonresonant contributions to the CARS signal. Spontaneous confocal Raman microscopy, on the other hand, records the full vibrational spectrum in each spot. It thus allows for subsequent background-free spectral analysis at every scanned spot. This is an important advantage, because, for example, spectral decomposition allows for separating and extracting various spectral components related to the presences of different materials in the confocal spot, which would be very difficult with CARS. Spontaneous confocal Raman microscopy, however, requires long measuring times, orders of magnitude larger than required for CARS.

We show here, employing spectral decomposition in the various regions of the vibrational spectrum that spatially resolved Raman microscopy at the single cell level can be used to simultaneously study nanoparticle uptake and their colocalization with intracellular compartments. Being strictly a label free technique, Confocal Raman Microscopy (CRM) [5, 6] thus is a valuable tool to study the interaction of NPs with biological matter at the cellular level. In this work we studied the uptake of CeO_2 and Al_2O_3 NPs, as well as of CNTs into Hepatocarcinoma cells by means of Confocal Raman Spectroscopy. The possibility of simultaneously detecting NPs together with the identification of their respective intracellular environment provided information about the three dimensional NP distribution in and their co-localization with different cell compartments, such as lipid bodies (LB), cytoplasm and nucleus.

2. Materials and Methods

2.1. Nanoparticles

2.1.1. *Metal oxide nanoparticles.* Al_2O_3 NPs were donated from PlasmaChem GmbH, Berlin, Germany. An average diameter between 2 and 5 nm was measured by TEM. CeO2 NPs were purchased from Evonik-Degussa GmbH. TEM studies revealed an average diameter of about 15 nm.

2.1.2. *Carbon Nanotubes (CNTs).* Multiwalled CNTs were purchased from Proforma (USA). To improve their stability in aqueous solutions CNTs were oxidised as described by Zhang et al. [7]. CNTs were sonicated with an ultrasonicator (SONICS® VCX 500) at 20% amplitude applying pulses of 30 seconds for 2 minutes to break the nanotubes into smaller pieces. After sonication TEM images showed an average length of 500 nm for the CNTs. Oxidized CNTs were silanized and endowed with initiator functionality for subsequent Atom Transfer Radical Polymerization (ATRP) following the method described by Llarena et al. [8]. Poly-sulfo propyl methacrylate (PSPM) was synthesized as a brush on the surface of CNTs (CNT/PSPM). The polyelectrolyte corona around the CNTs ensured stability in aqueous solution and served also as a support for the subsequent adsorption of a lipid layer. To this aim a layer of poly (allyl amine hydrochloride) (PAH) was assembled on top of the PSPM brush followed by adsorption of lipid vesicles composed of (1,2-Dioleoyl-sn-glycero-3-choline/1,2-Dioleoyl-sn-glycero-3-phospho-L-serine sodium salt) (DOPC/DOPS) in a molar ratio 3:1 [9].

2.2. Cell culture and NP exposure

The Hepatocarcinoma human cell line HepG2 (from American Type Culture Collection) was cultured in Dulbecco's Modified Eagle's Medium (DMEM) with 10% Fetal Bovine Serum (FBS), 1000 U

penicillin and 10 mg/ml streptomycin (all of them purchased from Sigma) at 37ºC and 5 % CO_2. When cell confluence reached around 70%, the culture was trypsinized and 100000 cells were seeded in glass bottom of Petri dishes. After 24 hours UV sterilized NPs were added to the Petri dishes. Details of the incubation protocol are the following: 50 µg/ml CeO_2 incubated for 48 h, 1 mg/ml Al_2O_3 NPs, 150 µg/ml CNTs/lipid and 50 µg/ml CNT/PSPM, all of them incubated for 24 h. Afterwards, the plate was rinsed with PBS several times and the cells were fixed with 3.7% formaldehyde in PBS during 30 minutes and rinsed again.

2.3. Confocal Raman Microscopy

Micro-Raman analyses were performed using a Renishaw inVia Raman Microscope. An excitation wavelength of 532 nm with a grating of 1800 mm^{-1} was used. Microspectroscopy measurements were conducted using the ×50 objective. The size of the focal spot was approximately 1 µm. Raman spectra were recorded from adherent cells placed into Petri dishes with a glass bottom filled with PBS. Spectra were measured in the region 300–3600 cm^{-1} with a resolution of approximately 7 cm^{-1}. The system was calibrated to the spectral line of crystalline silicon at 520.7 cm^{-1}. At least 8-20 accumulation scans in confocal mode at different spots in the various cell compartments were used to reduce the spectral noise. Control spectra of the different cell compartment were taken in different cells and averaged. All spectra were corrected for the PBS solution and Petri dish glass bottom baseline. After NPs exposure and repeated washings with PBS the Raman spectra were taken only from cells, where no visible NP aggregates could be observed.

3. Results and Discussion

Raman microspectroscopy allows for identification and localization of lipid bodies, cytoplasm and the nucleus in Hepatocarcinoma cells [10]. In brief, lipid bodies are identified by their strong CH_2 signal as compared with the CH_3 related bands. The nucleus shows a minimum intensity of CH_2 related vibrational bands, but comparatively intensive amide bands. In addition a specific nucleotide vibrational band can be seen, which is not present in the cytoplasm. Further details are given below.

3.1. Characteristic Raman spectra of NPs

Raman spectra of the two dried NPs and of the CNTs were recorded in non-confocal mode. Figure 1 represents the characteristic Raman spectra of CeO_2, Al_2O_3 NPs and CNTs.

CeO_2 NPs observed a single strong band located around 465 cm^{-1}. Cerium dioxide has a fluorite-type structure lattice and belongs to the space group O_h^5. Six optical-phonon branches of space group O_h^5 yield three zone center frequencies. The related triply degenerate Raman-active F_{2g} mode is centred at about 465 cm^{-1}. This mode represents a symmetric breathing vibrational mode of O ions around each cation [11]. It is rather sensitive to the oxygen sublattice disorder. One of the reasons of lattice disorder is a decrease of crystal dimensions. The Raman band shape of F_{2g} mode and their position thus change with decreasing size of NPs [12]. The corresponding wavenumber shift and asymmetrical broadening as a function of the crystal size can be theoretically described using the phonon confinement model [13]. The measured width of the F_{2g} mode of the studied CeO_2 NPs was about 8 cm^{-1} (Figure 1). Therefore the average size of the CeO_2 NPs can be estimated as about 18 nm. This value correlates very well with TEM studies of the used CeO_2 NPs.

Al_2O_3 belongs to the D_{3d} space group. From the 27 possible optical modes in the crystal structure of Al_2O_3 7 modes are Raman active and 6 modes are infrared (IR) active [14]. The seven arrows in Figure 1 denoted the seven Raman active modes in dried NPs. One of the IR active modes at 600 cm^{-1} can be also detected. This observation suggests a distorted microcrystalline structure of the NPs. Other bands observed in Al_2O_3 NPs can be assigned to the capping agent, which has been used by the supplier to avoid NP aggregation.

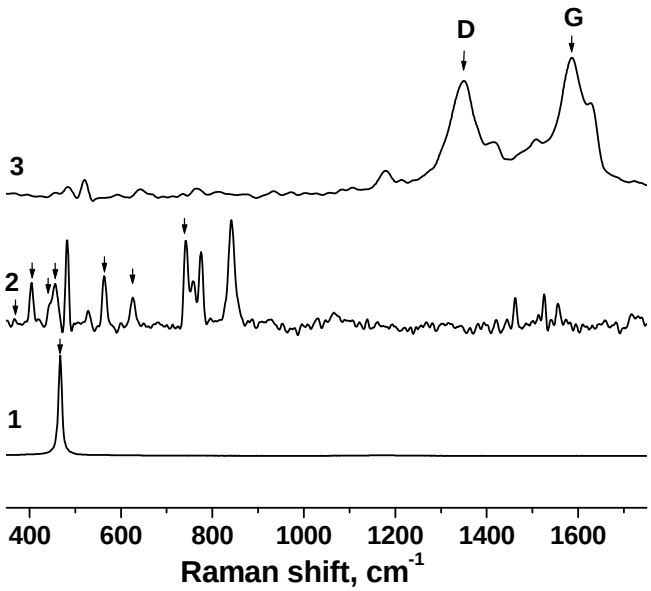

Figure 1. Raman spectra of CeO_2 (1), Al_2O_3 (2) and CNT (3) NPs.

The Raman spectrum of CNTs observes two prominent bands located at 1350 cm^{-1}, known as D-band, and at 1585 cm^{-1}, known as the G-band, see Figure 1. The D-band is an indicator for disorder in the graphene sheet and is also called "disorder-included" band. The G-band is a tangential mode originating from tangential oscillations of the carbon atoms in CNTs [15].

3.2. NPs localization in Hepatocarcinoma cells

The Raman spectra recorded from Hepatocarcinoma cells after their exposure to CeO_2, Al_2O_3 and CNT NPs all taken in confocal mode are shown in Figures 2, 3 and 4, respectively.

After exposure of the cells to CeO_2 Raman spectra were taken in various regions of the cells. Representative Raman spectra are displayed in Figure 2. They correspond to three different regions of the cell: lipid bodies, cytoplasm and nucleus. The assignments [5,16] of typical intracellular vibration bands are denoted in Figure 2. The three spectra reveal the different chemical nature of each of the chosen spots. The Raman spectrum in the lipid rich region was recorded from LBs, which can be seen in the microscopic transmission image as small spherical objects. The comparison of the spectra taken at different regions of the cell reveals that the intensity ratios of the CH_2 (2850 cm^{-1}) to the CH_3 (2935 cm^{-1}) symmetric stretching bands is much higher in LBs than in the cytoplasm or the nucleus, respectively. This follows from the considerably higher CH_2 group density in lipids than in proteins. The cytoplasmic compartment is characterized by a large amount of CH_3 groups and a comparatively small amount of lipids representing intracellular membranes. A comparison of the spectra in the cytoplasm and the nucleus shows some common bands, i.e. amid I (1655 cm^{-1}), and amid III (1250 cm^{-1}) bands, as well as different protein CH deformation modes. The band at 1338 cm^{-1} assigned to vibrations of adenine (A) and guanine (G) is quite specific for the nucleus and can be used to discriminate between cytoplasm and nucleus.

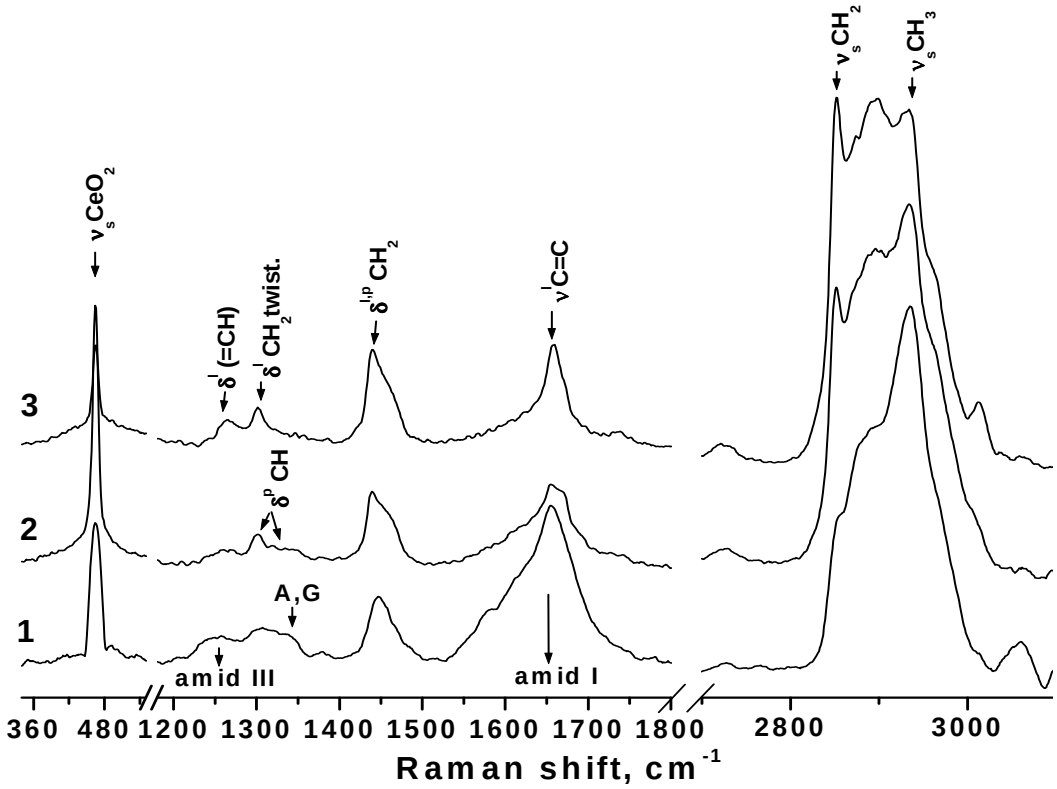

Figure 2. Raman spectra of cells exposed to CeO_2 NPs. The curves 1, 2 and 3 represent spectra recorded from different cell compartments: nucleus, cytoplasm and lipid bodies, respectively. The symbols ν and δ indicate stretching and deformation vibration modes, respectively. The indexes: l and p denote the vibrations of lipids and protein, respectively.

Regardless of the specific region of the cells in all spectra the CeO_2 phonon mode (465 cm^{-1}) was seen in parallel with the typical intracellular bands. This result demonstrates that CeO_2 NPs are distributed all over the cytoplasm. This does not necessarily mean that CeO_2 NPs enter the nucleus because NPs located just beneath or above the nucleus would contribute to the Raman spectra recorded from the nucleus. This is in agreement with the high but nevertheless limited spatial resolution of the confocal mode. A closer inspection reveals that the phonon band F_{2g} increases in its width to about 12 cm^{-1} after NPs uptake compared to pure NPs. From this follows an estimated NPs size of about 7 nm. This value is two times smaller compared to that of bare NPs. One of possible explanations may be that NPs with smaller sizes were preferentially taken by the cells. The other explanation is a relative dissolution of CeO_2 due to a relative reduction of Ce-IV atoms in Ce-III ones [17].

Figure 3 shows a Raman spectrum taken in a spot close to the nucleus of cell, which had been exposed to Al_2O_3 NPs. The typical seven Raman active bands resulting from Al_2O_3 in the low frequency region, denoted by arrows in Figure 3, were observed simultaneously with the signal from the cellular environment seen in the high frequency region. The pronounced CH_3 symmetric stretching band (2935 cm^{-1}) originated mainly from proteins. A weak lipid related CH_2 symmetric band indicates that the Al_2O_3 NPs were present in the cytoplasm being co-localized with proteins.

As a further example Figure 4 shows a spectrum recorded from cells treated with CNTs, which had been coated with lipids (CNT/lipid). Two characteristic vibrational bands of CNTs at 1350 cm^{-1} and 1585 cm^{-1}, D-band and G-band, can be clearly seen superimposed on the cellular spectrum. The spectrum can be decomposed into its two components, one from the CNTs and the other from the cell,

taking advantage of the spectrum of pure CNTs. After decomposition it was found that extracted cellular spectrum was very similar to spectra taken in the lipid-rich region of control cells. Clearly pronounced symmetric bands can be observed in the CH_2 stretching region. From the comparison of these spectra follows that lipid bodies and CNTs are both present within the 1 μm spot of the laser beam. From this observation one may conclude that lipid coated CNTs are likely colocalized with the lipid bodies in the cytoplasm. This may indicate a lipid facilitated way of uptake or an association with lipid bodies post uptake.

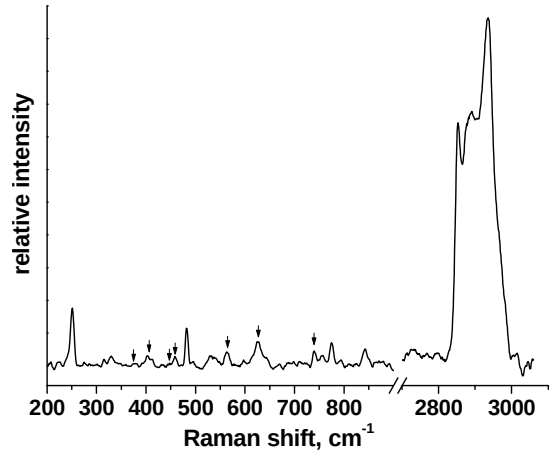

Figure 3. Spot Raman spectra taken close to the nucleus in cells exposed to Al_2O_3 NPs.

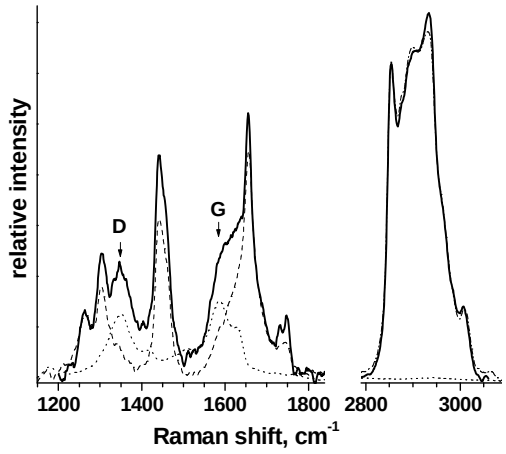

Figure 4. Spot Raman spectrum in cells exposed to CNT/lipid NPs (solid line). Dash and dot lines denote the contribution in recorded spectrum from NPs and LBs in cells, respectively.

In summary, it can be concluded that Raman spectra of NPs in cells do not only provide information about their presence but also on the intracellular environment in the vicinity of the nanoparticles.

3.3. NPs internalization and distributions across treated cells

In principle, confocal microscopy allows for the recording of Raman spectra in all three dimensions with an accuracy limited by the resolution of the device. However, since the signal intensity is small, a multidimensional spectral mapping would require a rather long time. Therefore, the spatial mapping was restricted to line scans in z-direction and in the xy-plane. The confocal resolution in z direction is not as good as that in the xy-plane. The accuracy in the z-direction is nevertheless sufficient to prove NPs internalization, but for colocalization studies it will be more appropriate to perform line scans in the xy-plane

Figures 5 and 6 show two examples of z-scans from cells exposed to CeO_2 NPs and CNTs covered with PSPM (CNT/PSPM). Z-scans were recorded in confocal mode along the z-axes with an increment of 2-5 μm. The z-plane denoted by zero is the reference plane assumed to be close to the equatorial plane of the cell. This plane was manually adjusted guided by imaging in transmission mode.

The signals from both CeO_2 NPs in low frequency region and from cells in the methyl/methylene stretching region can be seen in the z-scan spectra (Figure 5). The ratio between the phonon band intensity to the methyl/methylene band intensity depends on the z-plane. The maximum is found at z=5 μm. The pronounced lipid band at 2852 cm^{-1} evidences furthermore the colocalization of CeO_2 NPs with lipid-rich regions in the cell. From these z-scans clearly follows the internalization of the

CeO_2 NPs. The difference in intensity of the phonon band indicates an inhomogeneous distribution of the CeO_2 NPs within the cytoplasm.

In the case of cells exposed to CNT/PSPM both signals from NPs and cell were simultaneously recorded in the Raman spectra as observed in Figure 6. The typical D and G bands of the CNT were detected at different planes within the cells. The high intensity of the protein CH_3 stretching band and the apparent absence of lipid related Raman bands prove *i)* the cytoplasmic distribution of CNT/PSPM that the polyelectrolyte coated CNTs, together with *ii)* the absence of a specific affinity to the lipid body rich parts of the cytoplasm. As it can be seen the ratio between the signal intensity of the CNTs and that from the protein ($\nu_s(CH_3)$) is different for different planes. This implies that the CNTs are not homogeneously distributed in the cytoplasm.

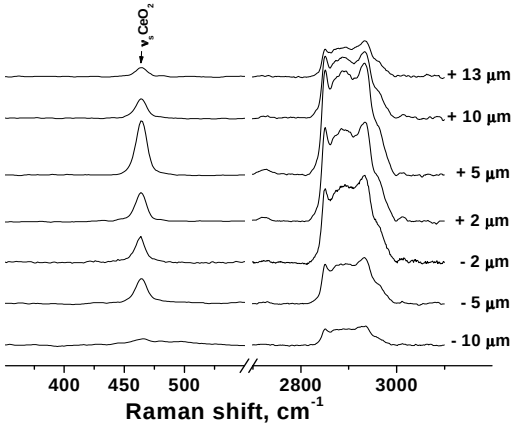

Figure 5. Raman spectra taken at different z-planes of the cell exposed to CeO_2 NPs

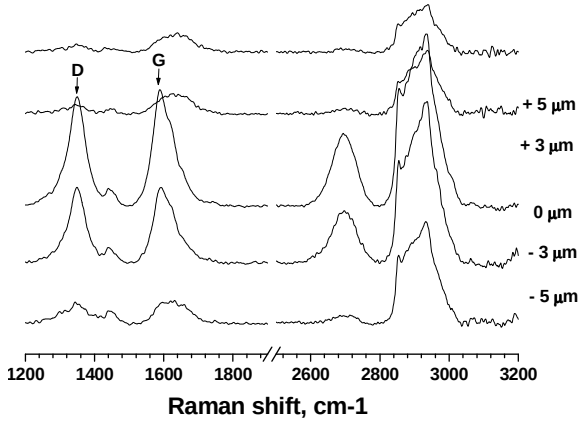

Figure 6. Raman spectra taken at different z-planes of the cell exposed to CNT/PSPM NPs

Line scans in the xy-plane of cells were performed to get more detailed information about the NPs distribution and their colocalization. Raman spectra were recorded along lines crossing through the exposed cells with a distance increment of 0.5 µm.

The recorded spectrum was decomposed into two components, one from the NPs and the other from the cell as outlined above (Figure 4). The relative integral intensities of the NP contribution in the Raman spectrum were calculated. The lipid CH_2 symmetrical stretching band at 2852 cm^{-1} was chosen as the reference band to obtain the lipid distribution along the scanned line. The integral intensities of $\nu_s(CH_2)$ was plotted as a function of the distance along the line. The lipid distribution across the cell reflects the presence of mainly lipid bodies. Other lipid fractions of the cytoplasm contribute to a lesser extent to the spectrum because their concentration is small compared with that of lipids in lipid bodies. A well pronounced maximum in the lipid distribution would thus indicate the presence of lipid bodies at this particular location.

Figure 7 displays the distributions of lipid bodies and NPs in cells exposed to CNTs, decorated with PSPM and to CNTs coated with lipids. For the purpose of displaying both distributions at the same graph in a comparable scale the component intensities of CNTs and cellular lipids were scaled to the intensity of a well pronounced maximum. The analysis revealed two regions where CNT/PSPM NPs concentration was large (Figure 7(a)). In the case of cells exposed to CNT/lipid NPs three maxima along the scan line in the xy-plane were found as shown in Figure 7(b). Of course, these maxima of the CNT distribution do not bear a specific relevance on its own. Only when compared to the lipid distribution conclusions may be drawn. Indeed, in Figure 7b all three maxima of the lipid distribution coincide with or are at least close to the maxima of the CNT distribution. This behaviour was regularly observed for cells exposed to lipid coated CNTs. In the case of CNT/PSPM NPs a spatial correlation between the localization of lipid bodies and the NPs was, however, not observed (Figure 7(a)). The lipid body intensity distribution had its maximum where the CNT signal intensity

lowest. That fact can be interpreted as a tendency of the CNT/PSPM NPs to avoid the site where the lipid bodies are preferentially located. These findings corroborate the conclusion drawn from Figure 4 that lipid coated CNTs within cells are found in close proximity of lipid bodies. This finding may point to either a lipid associated mechanism of uptake or to a retrospective arrangement of the CNTs with the lipid rich compartments in hepatocytes. In any case our finding suggests strongly that the nature of the surface of CNTs is important concerning their possible effects on cells.

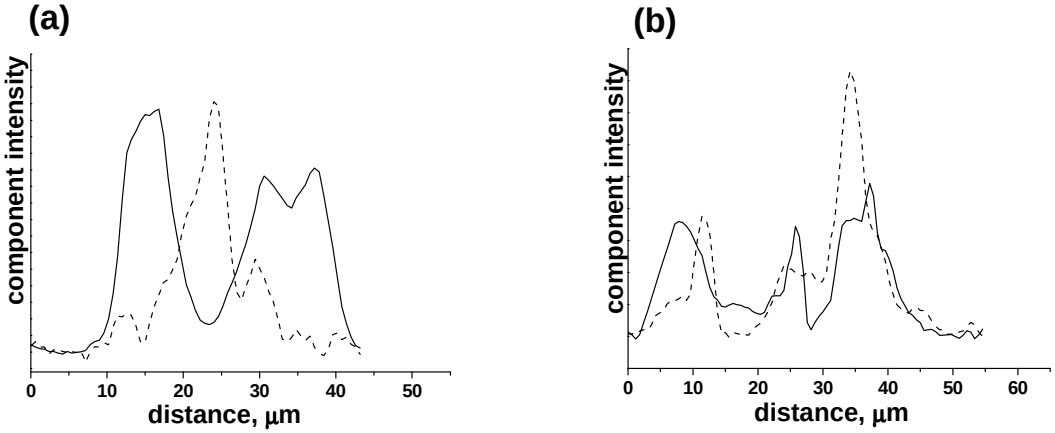

Figure 7. (a) CNT/PSPM, (b) CNT/lipids NPs distributions (solid lines) and lipids (dashed lines) distribution across CNT treated cell.

The analysis of a typical Raman microspectroscopy line scan after Al_2O_3 NPs exposure is shown in Figure 8. In this particular case the Al_2O_3 NPs were found close to the nucleus. The corresponding distributions of the components are presented as integral intensity distributions as well as in rainbow presentations overlaid on the transmission image. The protein distribution was calculated from the integral intensity of protein CH_3 stretching region as a function of distance along the line.

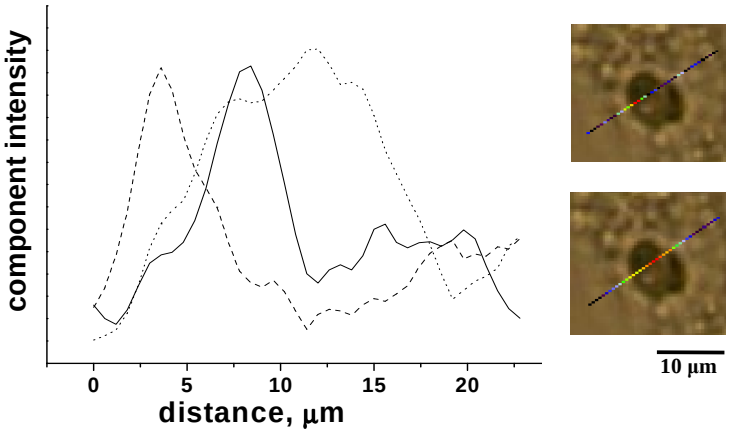

Figure 8. Al_2O_3 NPs (solid line), proteins (dot line) and lipids (dash line) distribution across the selected cell. The figure inserts represent NPs (top) and protein (bottom) line mapping overlaid on cell transmission images in rainbow presentation. The red colour corresponds to the maximum intensity.

The maximum of the protein distribution is correlated with the minimum of the lipid distribution. The maximum of the protein signal intensity or the minimum of lipid related signal intensity both could serve as a spectroscopic criterion of the nucleus position. The lower insert of Figure 8 proves that, for example, the protein signal intensity distribution is a good match of the optically observed nucleus as can be inferred from the overlap of the red dots with the optically dense nucleus region.

The analysis of lipid, protein and NPs distribution behaviour revealed the preferential association of the Al_2O_3 NPs with a protein rich region. The upper insert of Figure 8 displays an Al_2O_3 accumulation in the lower left sector close to the nucleus. On the other hand, maximum of NPs distributions differs by about 4 μm from the maximum of the protein related Raman signal, which is expected within the nucleus. From this analysis it most likely follows that in this particular case the Al_2O_3 NPs found along the line scan resided in the cytoplasm yet in a region close to nucleus. This conclusion is in agreement with the spectrum displayed in Figure 3, which in the same spot shows the signal from the Al_2O_3 NPs and the cytoplasm after Al_2O_3 NPs uptake.

4. Conclusions

It has been shown that Confocal Raman Microscopy is capable of providing detailed data on uptake and distribution of NPs in culture cells at single cell level. A specific advantage of the approach is that it does not require any labeling allowing in this way the investigation of the interaction of authentic nanoparticles with cells. Since most nanoparticles and nanomaterials observe Raman active vibration modes Confocal Raman Microscopy is a rather universal technique. The colocalization of nanoparticles with intracellular compartments can be elaborated applying spectral deconvolution. Another interesting aspect in the context of the interaction of nanoparticles with biological matter is that the size and surface composition of NPs has an influence on the phonon modes. This allows for monitoring changes in size and composition of nanoparticles while they are residing inside cells.

It was found that lipid coated CNTs associated preferentially with lipid bodies, while CNT/PSPM NPs avoided lipid-rich cell regions. This finding indicates that the surface properties of the nanoparticles may play a significant role concerning the uptake and intracellular distribution. Al_2O_3 and CeO_2 NPs were found in cytoplasm. The CeO_2 NPs signal was strong and found almost everywhere in the cytoplasm. This indicates a high rate of uptake of the latter and a non-specific distribution inside Hepatocarcinoma cells.

Acknowledgement

This work was supported by the European Commission in the framework of FP7 Theme 4 – NMP - Nanosciences, Nanotechnologies, Materials and New Production Technologies, Proposal No: CP-FP 28825-2 HINAMOX.

References

[1] Wardak A, Gorman ME, Swami N, Deshpande S 2008 *J Ind Ecol* **12** 435-48; Gwinn MR, Tran L 2010 *Wiley Interdiscip Rev Nanomed Nanobiotechnol* **2** 130-7; Tervonen T, Linkov I, Figueira JR, Steevens J, Chappell M, Merad M 2009 *J Nanopart Res* **11** 757-66; Schulte PA, Salamanca-Buentello F 2007 *Environ Health Perspect* **115** 5-12

[2] Maynard AD, Aitken RJ, Butz T, Colvin V, Donaldson K, Oberdorster G, Philbert MA, Ryan J, Seaton A, Stone V, Tinkle SS, Tran L, Walker NJ, Warheit DB 2006 *Nature* **444** 267-9; Gao XH, Cui YY, Levenson RM, Chung LWK, Nie SM 2004 *Nat Biotechnol* **22** 969-76; Oberdörster G, Maynard A, Donaldson K, Castranova V, Fitzpatrick J, Ausman K, Carter J, Karn B, Kreyling W, Lai D, Olin S, Monteiro-Riviere N, Warheit D, Yang H 2005 *Part Fibre Toxicol* **2** 8

[3] Hillegass JM, Shukla A, Lathrop SA, MacPherson MB, Fukagawa NK, Mossman BT 2010 *Wiley Interdiscip Rev Nanomed Nanobiotechnol* **2** 219-31; Lee J, Lilly GD, Doty RC, Podsiadlo P, Kotov NA 2009 *Small* **5** 1213-21

[4] Chan J, Fore S, Wachsman-Hogiu S, Huser T 2008 *Laser Photonics Rev* **2** 325-49; Moger J, Johnston BD, Tyler CR 2008 *Opt Express* **16** 3408-19; Tong L, Lu Y, Lee RJ, Cheng JX 2007 *J Phys Chem B* **111** 9980-5

[5] Puppels GJ, Demul FFM, Otto C, Greve J, Robertnicoud M, Arndtjovin DJ, Jovin TM 1990 *Nature* **347** 301-3; Deng H, Bloomfield VA, Benevides JM, Thomas GJ 1999 *Biopolymers* **50** 656-66; Chan JW, Taylor DS, Zwerdling T, Lane SM, Ihara K, Huser T 2006 *Biophys J*

90 648-56

[6] Chan JW, Lieu DK, Huser T, Li RA 2009 *Anal Chem* **81** 1324-31; Uzunbajakava N, Lenferink A, Kraan Y, Volokhina E, Vrensen G, Greve J, Otto C 2003 *Biophys J* **84** 3968-81; Takai Y, Masuko T, Takeuchi H 1997 *BBA-Gen Subjects* **1335** 199-208; Notingher I, Bisson I, Bishop AE, Randle WL, Polak JMP, Hench LL 2004 *Anal Chem* **76** 3185-93; Chernenko T, Matthaus C, Milane L, Quintero L, Amiji M, Diem M 2009 *ACS Nano* **3** 3552-9

[7] Zhang NY, Xie JN, Guers M, Varadan VK 2003 *Smart Mater Struct* **12** 260-3

[8] Llarena I, Romero G, Ziolo RF, Moya SE 2010 *Nanotechnology* **21** # 055605

[9] Fischlechner M, Zaulig M, Meyer S, Estrela-Lopis I, Cuellar L, Irigoyen J, Pescador P, Brumen M, Messner P, Moya S, Donath E 2008 *Soft Matter* **4** 2245-58; Moya S, Donath E, Sukhorukov GB, Auch M, Baumler H, Lichtenfeld H, Mohwald H 2000 *Macromolecules* **33** 4538-44

[10] Romero G, Estrela-Lopis I, Zhou J, Rojas E, Franco A, Espinel CS, Fernandez AG, Gao CY, Donath E, Moya SE 2010 *Biomacromolecules* **11** 2993-9

[11] Lacina WB, Pershan PS 1970 *Phys Rev B* **1** 1765-85

[12] Popovic ZV, Dohcevic-Mitrovic Z, Scepanovic M, Grujic-Brojcin M, Askrabic S 2011 *Annalen Der Physik* **523** 62-74; Weber WH, Hass KC, Mcbride JR 1993 *Phys Rev B* **48** 178-85; Kostic R, Askrabic S, Dohcevic-Mitrovic Z, Popovic ZV 2008 *Appl Phys A - Mater* **90** 679-83

[13] Richter H, Wang ZP, Ley L 1981 *Solid State Commun* **39** 625-9; Campbell IH, Fauchet PM 1986 *Solid State Commun* **58** 739-41

[14] Misra A, Bist HD, Navati MS, Thareja RK, Narayan J 2001 *Mat Sci Eng B-Solid* **79** 49-54; Porto SPS, Krishnan RS 1967 *J Chem Phys* **47** 1009-12

[15] Bose SM, Gayen S, Behera SN 2005 *Phys Rev B* **72** #153402; Keszler AM, Nemes L, Ahmad SR, Fang X 2004 *J Optoelectron Adv M* **6** 1269-74; Kuzmany H, Burger B, Hulman M, Kurti J, Rinzler AG, Smalley RE 1998 *Europhys Lett* **44** 518-24

[16] Peticolas WL. Raman Spectroscopy of DNA and Proteins. In: Biochemical Spectroscopy; 1995:389-416; Naumann D. Infrared and Raman spectroscopy of biological materials. New York: Marcel Dekker; 2001; Prescott B, Steinmetz W, Thomas GJ 1984 *Biopolymers* **23** 235-56

[17] Auffan M, Rose J, Orsiere T, De Meo M, Thill A, Zeyons O, Proux O, Masion A, Chaurand P, Spalla O, Botta A, Wiesner MR, Bottero JY 2009 *Nanotoxicology* **3** 161-U15